RESEARCH ARTICLE

Special Section:
East Asian Study of Tropospheric Aerosols and Impact on Cloud and Precipitation

Key Points:
- Taklimakan Desert dust can be lofted up to 10 km due to the unique topography
- The aerosol optical depth is significantly correlated with surface wind speed
- Two common synoptic features are favorable for dust emission and transport

Correspondence to:
J. P. Huang,
hjp@lzu.edu.cn

Characteristics of Taklimakan dust emission and distribution: A satellite and reanalysis field perspective

J. M. Ge[1], J. P. Huang[1], C. P. Xu[1,2], Y. L. Qi[1,3], and H. Y. Liu[1]

[1]Key Laboratory for Semi-Arid Climate Change of the Ministry of Education and College of Atmospheric Sciences, Lanzhou University, Lanzhou, China, [2]National Meteorological Center of China Meteorological Administration, Beijing, China, [3]College of Atmospheric Sciences, Chengdu University of Information Technology, Chengdu, China

Abstract Dust particles from the Taklimakan Desert can be lofted vertically up to 10 km due to the unique topography and northeasterly winds associated with certain synoptic conditions. Then they can be transported horizontally to regions far downwind by westerlies. We combined data from the Multiangle Imaging Spectroradiometer (MISR) and the Cloud-Aerosol Lidar with Orthogonal Polarization to investigate the three-dimensional distribution of dust over the Taklimakan Desert and surrounding areas. During spring and summer, a dust belt with high aerosol optical depths (AOD) extends eastward from the Taklimakan Desert to the Loess Plateau along the Hexi Corridor and southward to the Tibetan Plateau. However, the dust extinction coefficients decrease rapidly from $0.340\,km^{-1}$ near surface to $0.015\,km^{-1}$ at 5 km in spring, while the extinction values vary within 0.100 ± 0.020 between the altitudes of 1.6 and 3.5 km and decrease to $0.023\,km^{-1}$ at 5 km in summer, indicating that dust aerosol is relatively well mixed vertically. We further used MISR daily AOD to identify high- and low-dust days and then analyzed composite difference patterns of temperature, geopotential height, and wind between high- and low-dust days. It was found that although the synoptic situations of spring and summer are quite different, there are two common features: a strong anticyclonic wind anomaly over the Taklimakan at 500 hPa and an enhanced easterly wind over the Tarim Basin at 850 hPa for the two seasons. These conditions are favorable for dust entrainment from the dry desert surface, vertical lofting, and horizontal transport.

1. Introduction

Aeolian dust is lofted into the tropospheric boundary layer and above by strong surface winds associated with various weather systems ranging from synoptic scale cyclones to microscale turbulence. It has attracted great interest and become an important research topic in climate science [*Ge et al.*, 2008; *Huang et al.*, 2007a, 2008, 2010; *Kaufman et al.*, 2002; *Rosenfeld et al.*, 2001; *Tegen*, 2003]. Seasonal atmospheric processes, which modulate dust layer formation, have their own characteristics. Thus, the vertical and horizontal distributions and transport of dust aerosol can be quite variable in time and space. On a global, annual scale, lofted dust is the dominant aerosol in the atmosphere in terms of mass. The dust may directly impact the Earth's energy budget by scattering and absorbing solar radiation, absorbing and emitting thermal outgoing radiation, and indirectly influence clouds by acting as cloud condensation nuclei and ice nuclei to change the microphysical properties [*Bi et al.*, 2013; *Field et al.*, 2006; *Huang et al.*, 2006b; *Sassen et al.*, 2003; *Su et al.*, 2008; *Twohy et al.*, 2009]. As a light-absorbing aerosol [*Ge et al.*, 2010], dust can also heat the dust layer, change the thermal structure of atmosphere, evaporate clouds, and affect the hydrological cycle [*Chen et al.*, 2013; *Huang et al.*, 2009, 2006a; *Lau et al.*, 2006; *Ramanathan et al.*, 2001]. Therefore, dust can perturb the energy balance of the Earth-atmosphere system and affect radiative forcing on the climate system in complex ways. Earlier studies [*Claquin et al.*, 1998; *Ge et al.*, 2011; *Huang et al.*, 2009; *Liao and Seinfeld*, 1998] have shown that the magnitude of dust forcing is quite variable and the sign can be either positive or negative. This depends not only on the optical properties of dust but also on its horizontal and vertical distributions [*Haywood and Ramaswamy*, 1998]. Therefore, further analysis of the spatial and temporal variability of dust horizontal and vertical loading and optical properties is still needed to determine its effect on climate. The Taklimakan Desert is one of the largest global sources of atmospheric dust. It is located in the Tarim Basin (average elevation 1.1 km) in northwest China where it is bounded by the Pamir Plateau (average elevation 5.5 km) to the west and the Kunlun Shan range (average elevation 5.5 km) and Tian Shan range (average elevation 4.8 km) to the south and north,
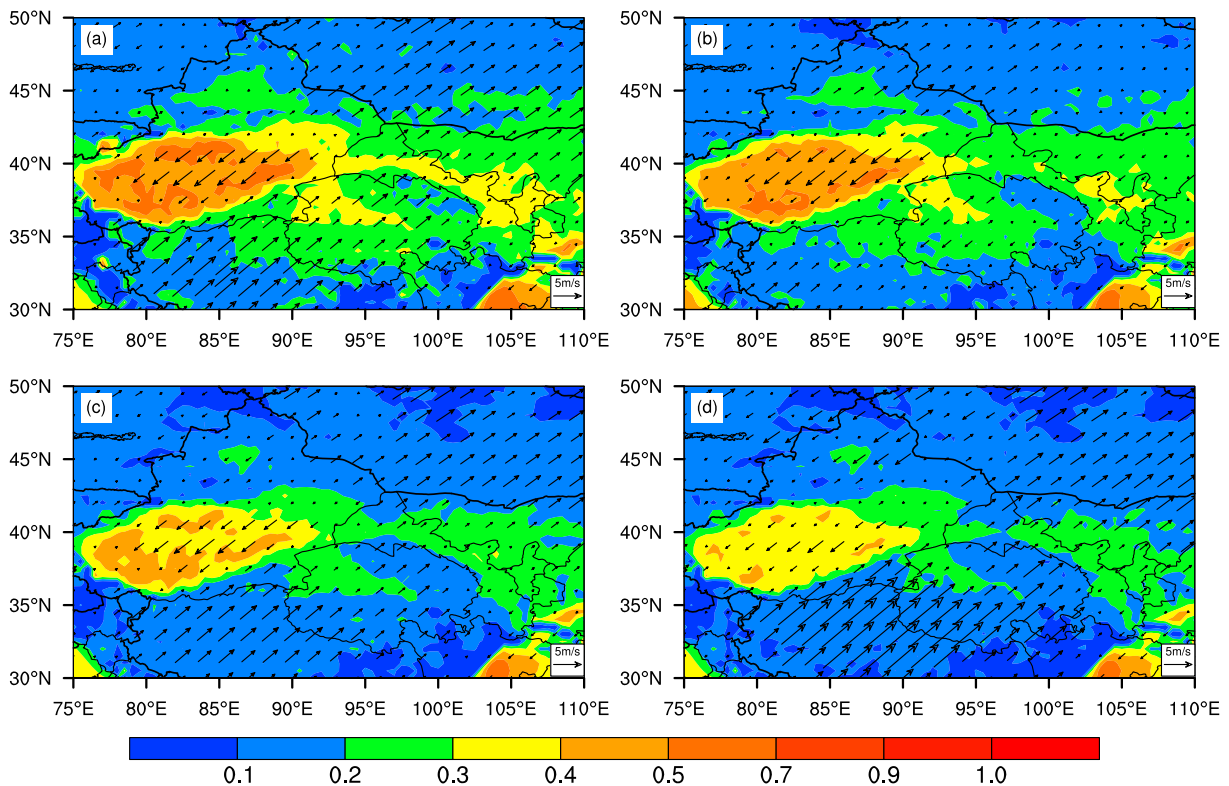
Figure 1. Seasonal mean MISR-based AOD along with 10 m winds for the years 2001 through 2012. (a) Spring, (b) summer, (c) autumn, and (d) winter.

respectively. The eastern margin of the Taklimakan is the only low-elevation opening for low-level dust to flow out of the desert basin. However, ERA-reanalysis data [*Dee et al.*, 2011] show that the low-level wind enters the Taklimakan through Lop Nur at the east side of the basin (see Figures 1 and 2). The prevailing transport wind direction, which is consistent with the direction of sand dunes motion in the desert [*Sun et al.*, 2001], is easterly and northeasterly almost all year long. Thus, dust layers lower than 5 km may not be easily transported out of this desert region. *Sun et al.* [2001] suggested that Taklimakan dust can be lofted to above 5 km, may persist for several days, and be transported for long distances. Using CALIOP (Cloud-Aerosol Lidar with Orthogonal Polarization) observations, *Huang et al.* [2007b] found that Taklimakan dust extended as high as 9 km in altitude and appeared over the Tibetan Plateau. Recently, case studies from CALIOP observations and aerosol transport model simulations have shown that Taklimakan dust was injected into the upper troposphere to altitudes of 4 to 10 km and transported more than one full circle around the global in about 13 days [*Eguchi et al.*, 2009; *Uno et al.*, 2009; *Yumimoto et al.*, 2009]. These studies, which are confined to individual or short-term dust events based on CALIOP data, reveal that Taklimakan dust can be lofted to the upper troposphere and transported to regions remote from the source areas. In this study, a climatological analysis of how this dust aerosol is distributed, horizontally as well as vertically, through the atmosphere above the Tarim Basin by seasons is investigated by using a multiyear database of CALIOP and MISR observations. MISR is a passive sensor that mainly provides column-integral aerosol information in the horizontal. When combined with CALIOP, an active lidar that can detect the vertical distribution of aerosol, the data provide unprecedented opportunity to study the three-dimensional characteristics of Taklimakan dust in more detail. Composite patterns of temperature, geopotential heights, and wind for days of high versus low dust loading were analyzed to understand the synoptic situations associated with dust outbreak and transport.

2. Data Sets

2.1. Terra-MISR

Since the first Earth Observing System (EOS) spacecraft Terra was successfully launched into a Sun-synchronous polar orbit in December 1999, MISR onboard Terra has performed continuously for over a
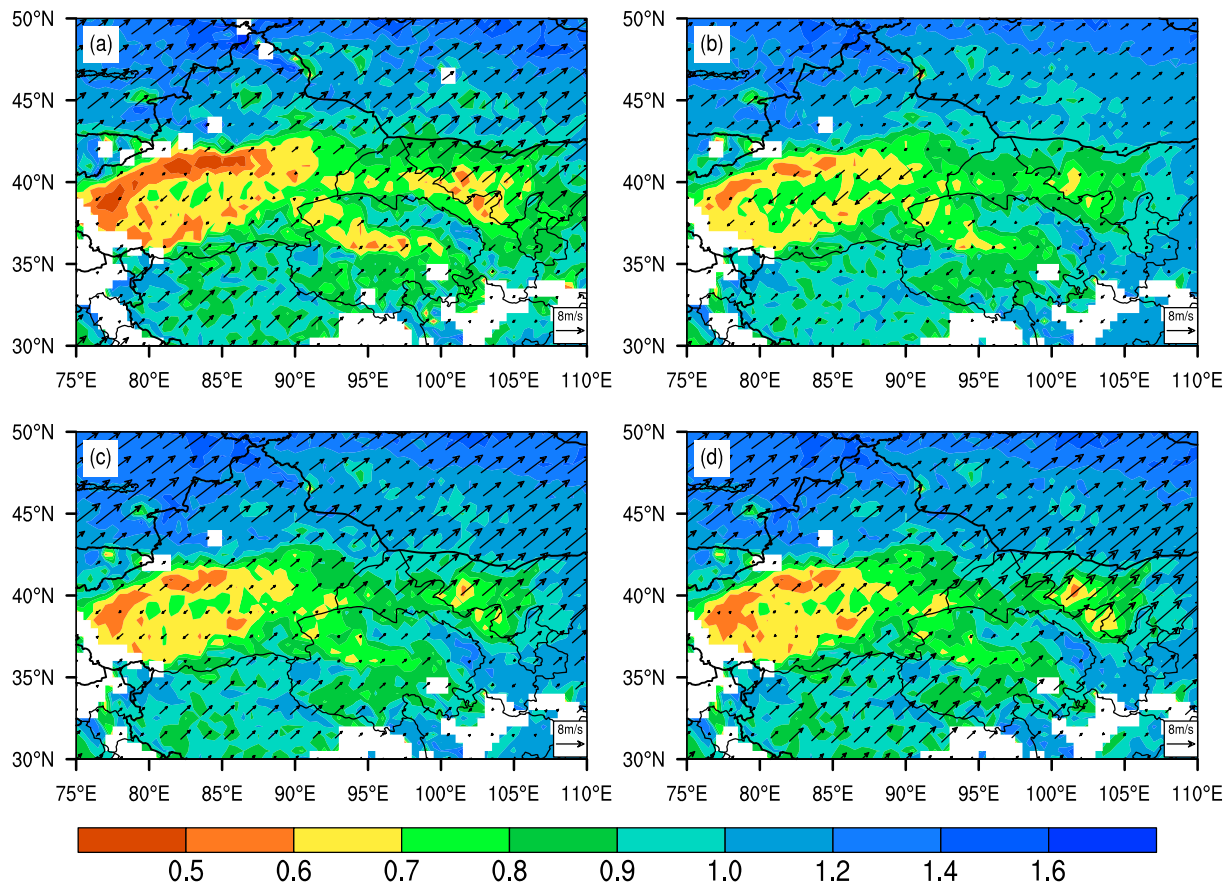
Figure 2. Seasonal mean MISR Ångström exponent along with 700 hPa winds for the years 2001 through 2012. (a) Spring, (b) summer, (c) autumn, and (d) winter.

decade. The MISR observations cover a swath approximately 360 km wide at the Earth's surface and obtain global coverage in about 9 days with a path-repeating cycle of 16 days. By taking advantage of the nine widely spaced angles, MISR can distinguish top-of-atmosphere reflectance contributions from the surface and atmosphere and successfully retrieve aerosol optical properties over bright surface such as the Taklimakan Desert [*Diner et al.*, 1998, 2005]. The spatial resolution of MISR level 2 aerosol data is 17.6 km by 17.6 km, which is used to produce level 3 data with the resolution of 0.5° by 0.5°. Here we used the level 3 daily Aerosol Optical Depth (AOD) data from January 2001 to December 2012. The Ångström exponent, which can be used as a qualitative indicator of aerosol particle size, is derived by a linear fit of natural logarithm of AODs versus wavelengths using the blue and green channels.

2.2. CALIPSO Lidar Measurement

CALIOP, which is the primary instrument aboard the CALIPSO (Cloud-Aerosol Lidar and Infrared Pathfinder Satellite Observations) launched in April 2006, is a near-nadir viewing (a small angle away from geodetic nadir to avoid strong specular lidar returns from still water and horizontally oriented ice crystals in clouds) two-wavelength polarization-sensitive lidar [*Winker et al.*, 2007, 2009]. It measures the backscattered laser signal at 532 and 1064 nm to acquire vertical profiles of cloud and aerosol information with a resolution of 333 m in the horizontal and 30 m in the vertical. The latest CALIOP version 3 level 2, 5 km cloud and aerosol layer products and the recently released version 1 level 3 globally gridded monthly aerosol profile data from 2006 through 2012 are used in this paper. CALIOP data are separated into day and night segments. Because of sunlight contamination, nighttime data are preferred due to a larger signal-to-noise ratio (SNR), and the lidar aerosol retrievals have higher accuracy than daytime signals. Level 2 layer data are used to statistically build the frequency of dust occurrence. Three steps of data screening are applied to the nighttime layer data in order to obtain high-quality results. We first examine the cloud layer product and identify those columns that have no cloud signal as cloud-free profiles. Then we select well-defined aerosol layers in the cloud-free profiles by

using the Cloud-Aerosol Discrimination score (CAD) as a parameter which represents the confidence level of cloud and aerosol discrimination: negative values for aerosol and positive values for cloud. A range of CAD scores between −100 and −50 is used to further screen the data. Third, in the selected layer data, the aerosol subtype identified as dust and the dust layer base height above the surface elevation are included in the final statistical description. This new level 3 aerosol product is produced from version 3 CALIOP level 2 aerosol profile data. All parameters in level 3 are quality screened prior to averaging on a 2° by 5° grid globally with 60 m vertical resolution. This screened, spatially averaged data set is used to construct monthly mean profiles of aerosol optical properties below 12 km. In addition to several quality control filters that have been adopted in level 3 data, we ignore the samples within 180 m of the maximum surface elevation in an attempt to remove surface contamination. We use nighttime combined (i.e., cloud-free + above-cloud) data to investigate the aerosol extinction profiles over the Taklimakan Desert and surrounding areas.

2.3. ERA-Interim Reanalysis

ERA-Interim is the latest global atmospheric reanalysis data set produced by the European Centre for Medium-Range Weather Forecasts (ECMWF). It provides data from 1979 onward and continues in real time. The products include a large variety of 3-hourly surface parameters, describing weather as well as ocean-wave and land-surface conditions, and 6-hourly upper air parameters covering the troposphere and stratosphere. Vertical integrals of atmospheric fluxes, monthly averages for many of the parameters, and other derived fields have also been produced. Substantial improvements have been archived in ERA-Interim by including many model improvements, such as the use of four-dimensional variation analysis, a revised humidity analysis, the use of variation bias correction for satellite data, and other improvements in data handling [*Dee et al.*, 2011]. The 6-hourly wind fields of 10 m and temperature, geopotential, and wind parameters on pressure levels from 2001 to 2012 were used here. The spatial resolution of the data is 1° by 1°.

3. Seasonal Structure of Taklimakan Dust

3.1. Spatial Distribution of Dust Loading

The seasonal dust burden, in terms of aerosol optical depth, and particle size, in terms of Ångström exponent, over the Taklimakan Desert and surrounding areas were investigated based on MISR observations. Figure 1 shows climatological means of AOD and near-surface wind speed and direction at 10 m height. It is clear that the surface wind direction is northeasterly and dust aerosol is prominent over the Tarim Basin all year long with the highest wind speed and AOD values occurring in spring and summer. In spring, a dust belt with high AOD extends eastward from the source region of the Taklimakan to the Loess Plateau along the north edge of the Tibetan Plateau and the Hexi Corridor. In summer, without cold front intrusions, the surface wind is not as strong as it is in spring; however, the mean AOD over the basin still can be as large as 0.7. We notice that there are two areas in the Tarim Basin where the AOD values are persistently greater than areas in the Taklimakan Desert, i.e., the northern and southern edges of the Tarim Basin. These two areas are along the southern foothills and slopes of the Tian Shan range and along the northern foothills of the Kunlun Shan range, respectively, where the topography may have strong local effects on wind strength, dust emission, and vertical motion.

Figure 2 shows the seasonally averaged Ångström exponent and winds at 700 hPa, i.e., a regional transport wind for comparison to surface winds. Compared to AOD in the two high-dust areas, the values of Ångström exponent in these areas are less than those in other areas, which indicate that the particle size of dust lofted in these areas is greater than that over the central region of the Taklimakan. *Gao and Washington* [2009] identified these two high dust-loading areas previously using the Total Ozone Mapping Spectrometer Aerosol Index measurements. Our loading results are consistent with their findings. However, they claimed that the dried river and lake beds left large amount of alluvial materials and sediments, which were very fine in size in these two areas, and that particles emitted from these two belts were thus likely to be very fine. This interpretation is shown to be incorrect by our data and analysis. By comparing Figures 1 and 2, we can see that during the spring and winter our AOD values over the northern area are similar to those over the southern edge, but in summer and autumn are less than those over the southern edge. However, the Ångström exponent values over the northern region are consistently less than those over the southern region during all four seasons. Both the northeasterly wind speeds and the surface grain size over the northern edge of the Tarim Basin are larger than those over the southern area [*Wang et al.*, 2002]. The stronger winds and larger particles can explain the smaller Ångström exponent values over the northern edge. Over the southern edge of the Tarim Basin, the Kunlun
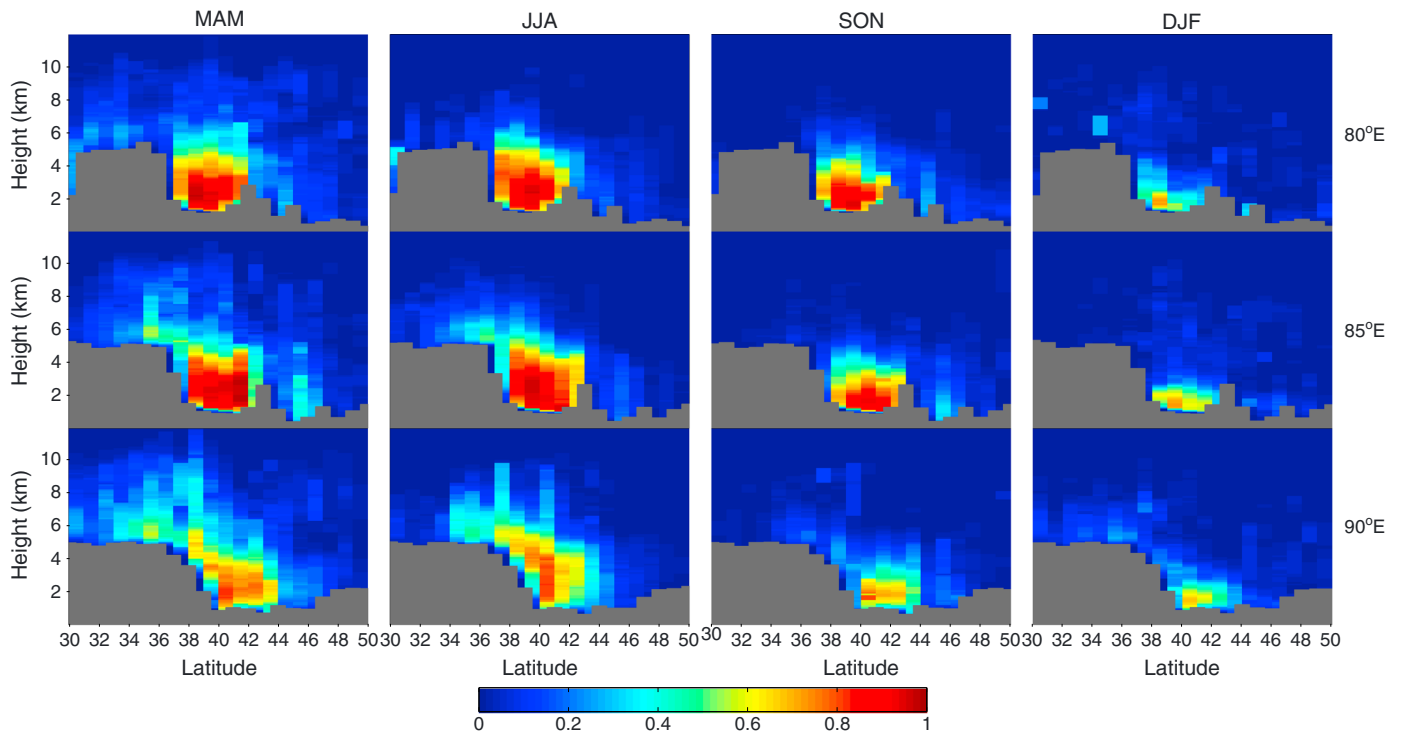
Figure 3. Seasonal dust occurrence frequency distribution over the Taklimakan Desert and surrounding areas for three longitudinal transects. Gray areas represent mountain profiles along the transects.

Shan range blocks the northeast winds and causes larger wind shear, which is a favorable condition for higher dust emissions. This may be a possible reason for the large dust loading over the southern area. We also note that the winds in the central part of the desert are stronger than those in the northern and southern areas. However, smaller AOD and larger Ångström exponent values occur over the central desert than over the other two regions for which there is no clear explanation.

3.2. Vertical Distribution of Dust

Since MISR is a passive sensor that can only provide measurements of column-integrated dust optical properties, we further use CALIOP levels 2 and 3 aerosol products to characterize the vertical distributions of the dust. Since CALIOP has a very narrow swath and a 16 day repeating cycle, the CALIOP level 3 aerosol product is produced by averaging samples into a global grid of 2° by 5° latitude-longitude boxes over month-long periods to provide global aerosol three-dimensional distributions. We selected a region from 77.5° to 87.5°E and 38° to 42°N to facilitate the intercomparison of CALIOP and MISR observations and represent aerosol over the Taklimakan Desert.

Figure 3 shows latitudinal transect plots of dust aerosol occurrences derived from CALIOP level 2 aerosol and cloud layer data. The dust occurrence frequency is defined as the ratio of the number of dusty profiles and the total number of valid profiles [*Liu et al.*, 2008]. The data for the three transect plots are averaged over regions of 1° of latitude between 30°N and 50°N, and over 5° of longitudes (2.5° on each side of central longitudes of 80°, 85°, and 90°E), and for the four seasons. These three longitudinal zones are selected to represent the vertical structure of dust over the western boundary, central region, and eastern entrance of the Tarim Basin. Generally, dust entrainment, lofting, and moderate to high loading are persistent during all seasons over this source region. The features of the vertical structure of the dust can be characterized in the following two ways. First, the height-resolved dust occurrence has an obvious seasonal variability. Dust occurs most frequently and over the greatest depth in spring and summer forming a layer from the surface that extends to altitudes of 8 to 10 km. Dust generation and lofting is less active during fall and winter and exhibits a lesser thickness, remaining primarily below 3 km in winter. Second, high dust occurrence can
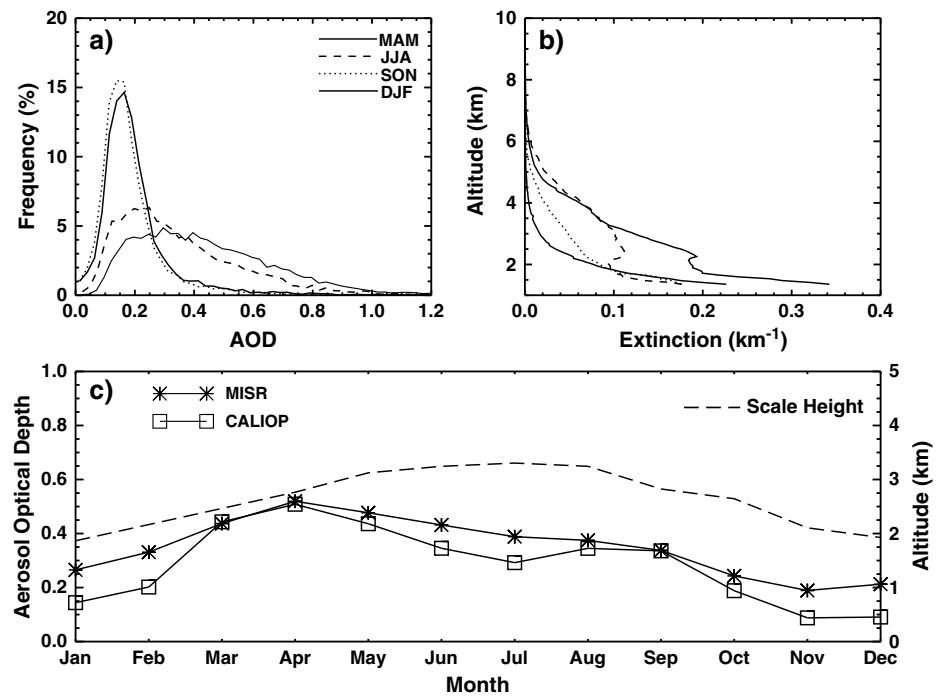
Figure 4. (a) Probability distribution function (PDF) of AOD from 12 years of MISR observations. (b) Seasonally averaged aerosol extinction profiles from 6 years of CALIOP observations. (c) Monthly mean of AOD values as measured by MISR and CALIOP during 2006 through 2012 and aerosol scale height.

extend from the bottom of the Tarim Basin to the Tibetan Plateau along the north slope of the Kunlun Shan range in spring and summer. This phenomenon is most clearly observed in the longitudinal cross sections of the central and eastern entrance of the Tarim Basin, 85° and 90°E transects, respectively. We may infer that the strong northeasterly surface winds blow into the Tarim Basin, entrain and loft dust particles, and transport this dust westward to the southern edge of the Tarim Basin until the flow is blocked by the Kunlun Shan range. Thus, the mountain slopes play an important role in the horizontal and vertical transport of the dust over the Tibetan Plateau and into the upper troposphere.

Figure 4a presents a histogram of the frequency of occurrence of AOD from 12 years of MISR data by season; Figure 4b shows the seasonal average aerosol extinction coefficient profiles derived from CALIOP; and Figure 4c compares the monthly AODs average between 6 years of MISR and CALIOP observations from June 2006 to May 2012 along with the aerosol scale height from Figure 4b. In Figures 4a and 4b one can see that the column-integrated AOD and extinction profile values in spring and summer are much greater than those during the other two seasons. The largest extinction value of $0.34\,km^{-1}$ appears near the surface in spring; however, in that season the extinction coefficients decrease more rapidly with height to $0.015\,km^{-1}$ at 5 km. In summer, the near-surface dust aerosol extinction is lower but the aerosol is uniformly mixed in the vertical. The extinction value varies within $0.1 \pm 0.02\,km^{-1}$ between the altitudes of 1.6 and 3.5 km and decreases to $0.023\,km^{-1}$ at 5 km. The monthly averaged CALIOP AODs are integrated from the corresponding average extinction profiles and shown in Figure 4c. The seasonal variation of CALIOP-based AOD compares well with MISR AOD. The lowest dust AOD value appears in November with similar values in December and January and then increases, reaching the highest values of about 0.45 in the spring months of March through May and peaking in April, which is the most active month for dust storms in China when cold air outbreaks from the northwest occur most frequently [*Sun et al.*, 2001]. The CALIOP AOD values are less than MISR AODs in months other than March, April, and September when they are essentially equal. Keep in mind that the highest dust loadings due to dust transported to the upper troposphere may be misclassified as clouds by CALIOP, which would result in a low bias to CALIOP aerosol extinction values. Other possible reasons for these differences may be the AOD retrievals of MISR or CALIOP, data screening and averaging methods, or diurnal variation of aerosol loading. (Note that MISR observes aerosol during the daytime, while CALIOP observations are sampled at night in this study.)
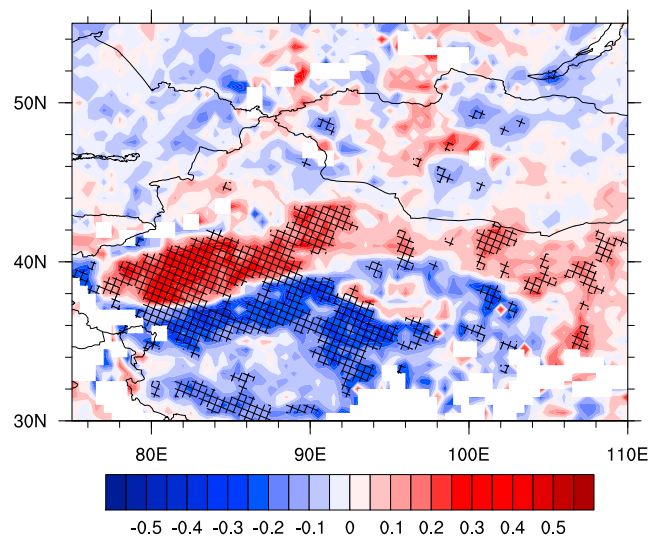
Figure 5. Correlations between AOD and 10 m winds velocity for the period of 2001 through 2012. The cross-hatched area represents the locations where the correlation coefficients are significant at the 95% confidence level.

We also calculated the monthly mean aerosol scale height and have plotted it along with AODs in Figure 4c. The aerosol scale height is defined as that altitude below which 63% of the AOD occurs [*Yu et al.*, 2010]. This is a simple and useful parameter to describe aerosol vertical distribution and characterize the strength of vertical transport in the aerosol source region. The monthly mean value of the aerosol scale height varies from 1.9 to 3.3 km and has an apparent seasonal cycle over the Taklimakan Desert. During the spring months (MAM; March-April-May) aerosol scale heights vary from 2.5 to 3.1 km. The mean value is 3.2 km in summer reaching the highest altitude of 3.3 km in July and then beginning a steady decrease in August. In winter the aerosol scale heights are several hundred meters above the mean surface level (1.5 km) with the lowest value of 1.9 km in January over this region. The combined plot of AOD and aerosol scale height illustrates that most dust aerosols generated in spring are concentrated in the lower atmosphere. In summer, dust layers extend higher in the troposphere, and during autumn and winter the dust aerosol is generally confined to the boundary layer.

4. Large-Scale Atmospheric Circulation and Dust Loading

Dust emission is related to complex processes which are governed and modulated by meteorology and properties of land surfaces such as soil composition, soil grain size, vegetation cover, and soil moisture [*Ginoux et al.*, 2001; *Knippertz and Todd*, 2012; *Shaw et al.*, 2008]. Considering that there is sparse vegetation and little annual precipitation and that the geomorphology of the desert surface is generally uniform and continuous over the Tarim Basin, dust concentration should be highly correlated with near-surface wind speed. The MISR daily AOD data were averaged over 1° by 1° units to match the ERA-Interim near-surface (10 m) wind series of each grid element. The ERA-Interim wind speeds at 0000 UTC (roughly 4 h prior to MISR overpass) were used. The areas over which correlation coefficients between MISR AOD and ERA wind speed are plotted in Figure 5. It is interesting to note that there is a strong positive relationship between AOD and wind speed over the Taklimakan Desert and surrounding areas. Positive correlations appear over the Taklimakan, in the Hexi Corridor, and over the Loess Plateau, and the correlations become negative over the Tibetan Plateau except over the Qaidam Basin, which is a desert region on the northern side of the plateau. Without considering soil moisture, vegetation, etc., it is straightforward to expect that stronger winds will entrain, loft, and suspend more dust particles over the dust source regions and therefore cause the positive correlation.

As shown in Figure 3, an area of high dust occurrence appears over the region of lowest elevation in the Tarim Basin toward the Tibetan Plateau along the north slope of the Kunlun Shan range and extends south to a latitude of about 34°N. Although there are some areas of high dust occurrence over the Tibetan Plateau, the correlations are generally negative over this region and are statistically significant at the 95% confidence level. Our explanation is that dust from the Taklimakan Desert is continuously transported toward up and over the Tibetan Plateau. However, if local, low-level winds over Tibetan Plateau are strong, these dust particles will be rapidly dispersed; otherwise, when local wind speeds are weaker, dust aerosol will tend to accumulate over the Tibetan Plateau. We also note that over the southern part of the Tibetan Plateau, winds are negatively correlated with AOD. These correlations, although not high, are statistically significant. A previous study [*Liu et al.*, 2008] has shown that dust particles from the Arabian Peninsula and Indian Subcontinent can be transported to the southern side of Tibetan Plateau. That may be another reason that

Figure 6. (a and b) Composite differences of temperature, (c and d) geopotential height, and (e and f) wind in spring season during 2001 through 2012. Figures 6a, 6c, and 6e are for 850 hPa, and Figures 6b, 6d, and 6f are for 500 hPa. The stippled area represents the 95% confidence level.

winds have an inverse relationship with AOD over this area. Since dust emission, transport, and distribution are primarily controlled by synoptic-scale meteorology, we further examined large-scale composite patterns of wind and geopotential heights for high dust-loading days versus those for low dust-loading days in spring and summer seasons. We first defined the "background" AOD as the MISR AOD value corresponding to the maximum of AOD probability distribution function (PDF) shown in Figure 4a. For example, the background AOD values for spring and summer are 0.29 and 0.21, respectively. Then we identified the low dust-loading days as those days when the median value of daily AOD over the Taklimakan was not larger than the background values. Note that the background AOD values of spring and summer correspond to a value about 20% of the daily AOD median value cumulative distribution function (CDF). Thus, we select the AOD values at the 80% of the median value of the CDF, which are 0.65 and 0.57 for spring and summer, respectively, as the threshold for identifying high dust-loading days. Applying this criterion, 95 high and 99 low dust-loading days in spring, and 109 and 104 days, respectively, in summer were selected.
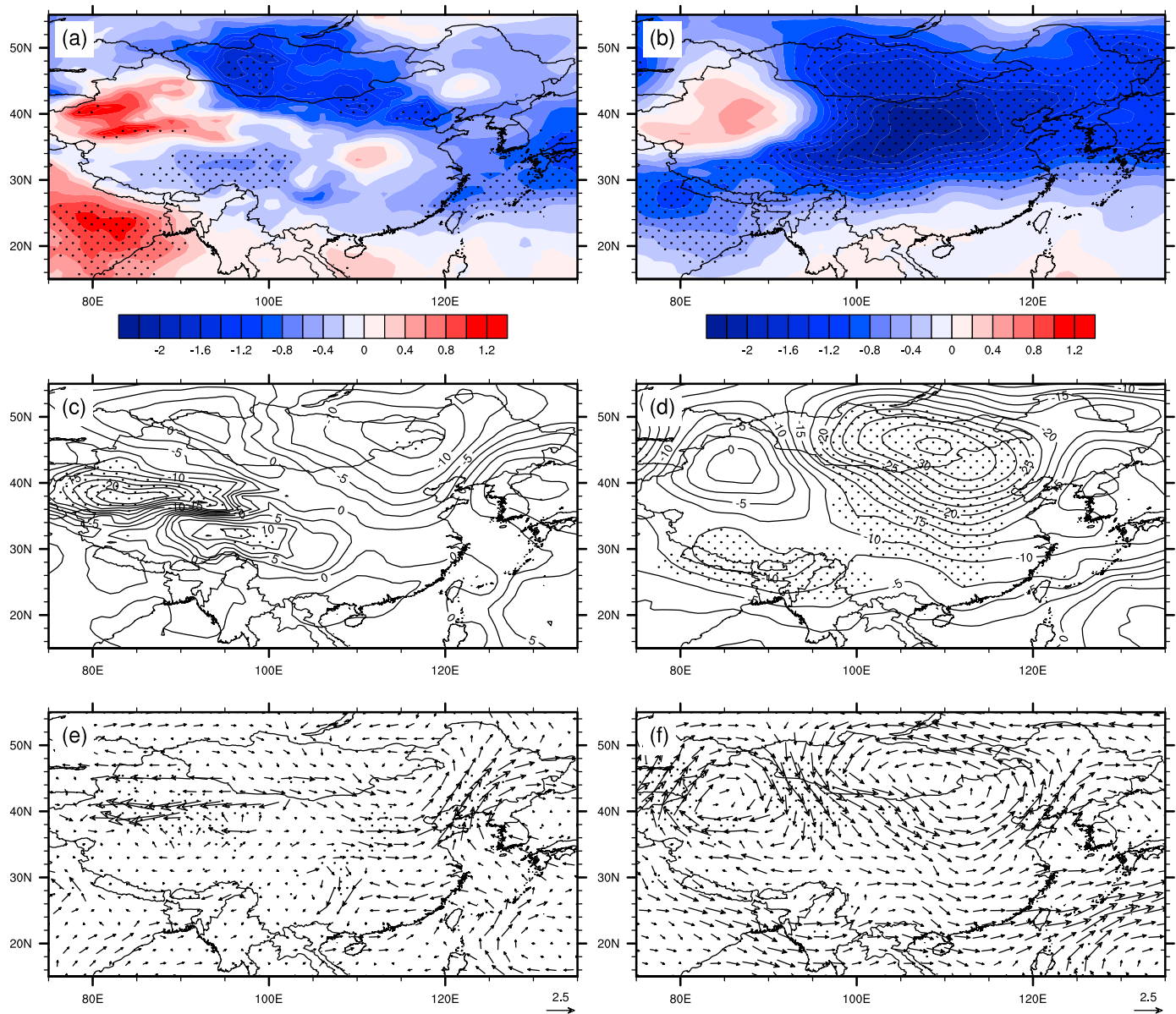
Figure 7. Same as in Figure 6 but for summer season.

Figures 6 and 7 show the composite difference patterns of temperature, geopotential height, and wind flow fields between high- and low-dust days at 850 hPa and at 500 hPa for spring and summer seasons, respectively. In spring, a positive temperature difference covers most parts of northern China. A kernel of greater than 4° is centered over Northeast China (46°N, 127°E) at 850 hPa (Figure 6a); this positive region is still obvious at 500 hPa with the core shifting eastward to 46°N, 135°E (Figure 6b). There is another distinct relative warm core of 4°C located at 39°N, 90°E at the 500 hPa level. Corresponding to the two relative warm regions, there are two closed high centers, one with a +50 geopotential meter (gpm) difference centered about 48°N, 90°E, and a second with +60 gpm difference at about 46°N, 135°E on 500 hPa level. These enhanced geopotential heights cause two strong regions of anomalous anticyclonic flow at 500 hPa as shown in Figure 6d. The related anomalous winds occurring to the south of 48°N will weaken the intensity of the normal westerly flow, which is favorable for dust transport and vertical mixing. At 850 hPa, there is a region with anomalous positive geopotential height over Mongolia. The geopotential height differences over the Tarim Basin and Inner Mongolia have negative values of about −10 gpm. A strong geopotential height anomaly gradient along the China-Mongolia border to the Tarim Basin will cause significant

enhancement of northeasterly and easterly winds into and over the Taklimakan Desert and thus tend to entrain and loft greater amounts of dust into the atmosphere.

The summer features of the temperature and geopotential height composite difference fields in Figure 7 are unlike those in spring. The temperature difference field at 850 hPa shows a warm area over the western Tarim Basin and cool areas from Mongolia southeastward toward North China and also over the Tibetan Plateau. A weak relative warming of about 0.4°C is present over the east entrance of the Taklimakan Desert, and a significant negative temperature difference region is located to the east of the Tarim Basin between 30°N and 50°N at 500 hPa. A significant negative geopotential height difference region with a central value less than −30 gpm covers most of Mongolia and Inner Mongolia at 500 hPa. To the west of this low, a weak high is centered over the Taklimakan Desert and causes a strong, northeasterly gradient between the low and high centers. Thus, we can see an enhancement of anticyclonic winds over the Tarim Basin with a significantly increased northeasterly and easterly wind component of up to 4 m/s over the east entrance of the Tarim Basin and the Taklimakan Desert, respectively. On the 850 hPa surface, a significant negative geopotential height difference region that dominates the Tarim Basin with a central value of about −20 gpm lies close to the northern edge of the Tibetan Plateau. This southward geopotential height anomaly gradient leads to a significant enhancement of easterly winds between 38°N and 42°N over the Tarim Basin, and thus, dust still can be lofted up into atmosphere during the summer time.

5. Discussion and Conclusion

We used the 12 year (2001 through 2012) MISR data set to identify days of relatively high and low dust loading and investigate the resulting geographical and seasonal distribution of optical depth and particle size over the Taklimakan Desert and surrounding areas. Similarly, we used the 6 year (2006 through 2012) CALIOP data set to characterize the vertical extinction profile and vertical distribution of desert dust over the same region. ERA-Interim reanalysis data were used to analyze the composite of synoptic patterns between days of high and low dust loading that were identified by MISR daily AOD observations.

Events of dust entrainment and lofting are most frequent and active during spring and summer over the Tarim Basin. The AODs in a belt over the northern and southern edges of the Tarim Basin are persistently greater than those over the central Taklimakan Desert and the areas surrounding the belt. Ångström exponent values are smaller over the belt, which indicates that the mean effective radius of the particle size distribution over these high AOD areas is larger than that over the central Taklimakan. The prevailing wind directions at low and middle levels are easterly and northeasterly nearly all year long; thus, the dust layer below 5 km altitude may be hemmed in by the 5 km or higher surrounding topography and may not be easily advected out of the Taklimakan region. The CALIOP measurements show that height-resolved dust occurrence frequencies have higher values in spring and summer, extending to the upper troposphere, and the lower values in fall and winter that are mainly limited to within the boundary later. We also find that significant amounts of dust can be lofted from the bottom of the Tarim Basin (~1.5 km elevation) up to the Tibetan Plateau (~5 km and higher) along the north slope of the Kunlun Shan range in spring and summer. Here we also provided the seasonally averaged aerosol extinctions and scale heights. The extinction coefficients during spring and summer are greater than those in the other seasons. In spring, dust extinction coefficients peak near the surface with a value of $0.34 \, km^{-1}$ and decrease rapidly to $0.015 \, km^{-1}$ at 5 km, while in summer the extinction coefficient varies within 0.1 ± 0.02 between 1.6 and 3.5 km and decreases slowly to $0.023 \, km^{-1}$ at 5 km. The CALIOP column-integrated AOD compares well with MISR AOD. Both exhibit the lowest AOD in November and largest in April. The aerosol scale height in spring varies from 2.5 to 3.1 km. This parameter increases in summer with a peak of 3.3 km in July and decreases through winter when the minimum of 1.9 km appears. From the analysis of AOD and scale height, we can conclude that most of the dust emissions are concentrated in the lower atmosphere in spring, are lofted to higher levels in summer and fall, and in winter they are mainly confined to the boundary layer.

The MISR-based AOD values are highly correlated to surface winds with positive correlations over the Tarim Basin and negative correlations over the Tibetan Plateau. This relationship occurs because stronger winds over the dust source region will generate and loft more dust, while stronger winds over the Tibetan Plateau may more rapidly dilute and disperse dust that was transported from the basin. The temperature, geopotential height, and wind field differences between high and low dusty days for spring and summer

were also analyzed to understand the synoptic meteorology of these seasons and the mechanisms of dust injection and transport. In spring, there are two relative warm regions at 500 hPa centered at 48°N, 90°E, and 46°N, 135°E, respectively. These are nearly the same areas where two high-pressure anomalies appear in the geopotential fields with central difference values of +50 gpm and +60 gpm. These phenomena suggest that the mean Xinjiang high-pressure ridge which normally appears at midlevel and low level in spring [*Liu et al.*, 2004] becomes stronger, while the mean Sea of Japan troughs become weaker. These anticyclonic anomalies also weaken the westerly flow. Moreover, a strong geopotential height anomaly gradient exists between the China-Mongolia border and the Tarim Basin at 850 hPa and thus enhances northeasterly and easterly winds into the Taklimakan, lofting large amounts of dust into the air. The situation during summer time is quite different. At 500 hPa, a significant mean low with a central anomaly of −30 gpm and a weak high system are located over Mongolia and Inner Mongolia, and the Taklimakan, respectively. Between them a steep gradient of geopotential heights exists causing an enhancement of anticyclonic flow over the Tarim Basin with increasing northeasterly and easterly winds. At 850 hPa, a relatively warm anomaly is located over the Tarim Basin and a cool anomaly extends from Mongolia to North China. The stronger geopotential height gradient due to this anomaly near the north edge of the Tibetan Plateau strengthens easterly winds, lofts, and transports dust out of the Tarim Basin. From our study we may imply that the high concentrations of particles lofted from the Taklimakan can interact with ice clouds, and dust deposits on the Tibetan Plateau can change the snow surface albedo and increase the snow melt, thus will affect climate change. It is also expected that the response of synoptic conditions to climate change could affect the dust aerosol emission and distribution over this region.

References

Bi, J., J. Huang, Q. Fu, J. Ge, J. Shi, T. Zhou, and W. Zhang (2013), Field measurement of clear-sky solar irradiance in Badain Jaran Desert of Northwestern China, *J. Quant. Spectrosc. Radiat. Transfer*, *122*, 194–207.

Chen, S., J. Huang, C. Zhao, Y. Qian, L. R. Leung, and B. Yang (2013), Modeling the transport and radiative forcing of Taklimakan dust over the Tibetan Plateau: A case study in the summer of 2006, *J. Geophys. Res. Atmos.*, *118*, 797–812, doi:10.1002/jgrd.50122.

Claquin, T., M. Schulz, Y. Balkanski, and O. Boucher (1998), Uncertainties in assessing radiative forcing by mineral dust, *Tellus B*, *50*, 491–505.

Dee, D. P., et al. (2011), The ERA-Interim reanalysis: Configuration and performance of the data assimilation system, *Q. J. R. Meteorol. Soc.*, *137*, 553–597.

Diner, D. J., et al. (1998), Multi-angle Imaging SpectroRadiometer (MISR)—Instrument description and experiment overview, *IEEE Trans. Geosci. Remote Sens.*, *36*, 1072–1087.

Diner, D. J., J. V. Martonchik, R. A. Kahn, B. Pinty, N. Gobron, D. L. Nelson, and B. N. Holben (2005), Using angular and spectral shape similarity constraints to improve MISR aerosol and surface retrievals over land, *Remote Sens. Environ.*, *94*, 155–171.

Eguchi, K., I. Uno, K. Yumimoto, T. Takemura, A. Shimizu, N. Sugimoto, and Z. Liu (2009), Trans-Pacific dust transport: Integrated analysis of NASA/CALIPSO and a global aerosol transport model, *Atmos. Chem. Phys.*, *9*, 3137–3145.

Field, P. R., O. Moehler, P. Connolly, M. Kraemer, R. Cotton, A. J. Heymsfield, H. Saathoff, and M. Schnaiter (2006), Some ice nucleation characteristics of Asian and Saharan desert dust, *Atmos. Chem. Phys.*, *6*, 2991–3006.

Gao, H., and R. Washington (2009), The spatial and temporal characteristics of TOMS AI over the Tarim Basin, China, *Atmos. Environ.*, *43*, 1106–1115.

Ge, J., J. Huang, F. Weng, and W. Sun (2008), Effects of dust storms on microwave radiation based on satellite observation and model simulation over the Taklamakan Desert, *Atmos. Chem. Phys.*, *8*, 4903–4909.

Ge, J. M., J. Su, T. P. Ackerman, Q. Fu, J. P. Huang, and J. S. Shi (2010), Dust aerosol optical properties retrieval and radiative forcing over northwestern China during the 2008 China-US joint field experiment, *J. Geophys. Res.*, *115*, D00K12, doi:10.1029/2009JD013263.

Ge, J. M., J. P. Huang, J. Su, J. R. Bi, and Q. Fu (2011), Shortwave radiative closure experiment and direct forcing of dust aerosol over northwestern China, *Geophys. Res. Lett.*, *38*, L24803, doi:10.1029/2011GL049571.

Ginoux, P., M. Chin, I. Tegen, J. M. Prospero, B. Holben, O. Dubovik, and S. J. Lin (2001), Sources and distributions of dust aerosols simulated with the GOCART model, *J. Geophys. Res.*, *106*, 20,255–20,273, doi:10.1029/2000JD000053.

Haywood, J. M., and V. Ramaswamy (1998), Global sensitivity studies of the direct radiative forcing due to anthropogenic sulfate and black carbon aerosols, *J. Geophys. Res.*, *103*, 6043–6058, doi:10.1029/97JD03426.

Huang, J., B. Lin, P. Minnis, T. Wang, X. Wang, Y. Hu, Y. Yi, and J. K. Ayers (2006a), Satellite-based assessment of possible dust aerosols semi-direct effect on cloud water path over East Asia, *Geophys. Res. Lett.*, *33*, L19802, doi:10.1029/2006GL026561.

Huang, J., P. Minnis, B. Lin, T. H. Wang, Y. H. Yi, Y. X. Hu, S. Sun-Mack, and K. Ayers (2006b), Possible influences of Asian dust aerosols on cloud properties and radiative forcing observed from MODIS and CERES, *Geophys. Res. Lett.*, *33*, L06824, doi:10.1029/2005GL024724.

Huang, J., J. Ge, and F. Weng (2007a), Detection of Asia dust storms using multisensor satellite measurements, *Remote Sens. Environ.*, *110*, 186–191.

Huang, J., P. Minnis, Y. Yi, Q. Tang, X. Wang, Y. Hu, Z. Liu, K. Ayers, C. Trepte, and D. Winker (2007b), Summer dust aerosols detected from CALIPSO over the Tibetan Plateau, *Geophys. Res. Lett.*, *34*, L18805, doi:10.1029/2007GL029938.

Huang, J., P. Minnis, B. Chen, Z. Huang, Z. Liu, Q. Zhao, Y. Yi, and J. K. Ayers (2008), Long-range transport and vertical structure of Asian dust from CALIPSO and surface measurements during PACDEX, *J. Geophys. Res.*, *113*, D23212, doi:10.1029/2008JD010620.

Huang, J., Q. Fu, J. Su, Q. Tang, P. Minnis, Y. Hu, Y. Yi, and Q. Zhao (2009), Taklimakan dust aerosol radiative heating derived from CALIPSO observations using the Fu-Liou radiation model with CERES constraints, *Atmos. Chem. Phys.*, *9*, 4011–4021.

Huang, J., P. Minnis, H. Yan, Y. Yi, B. Chen, L. Zhang, and J. K. Ayers (2010), Dust aerosol effect on semi-arid climate over Northwest China detected from A-Train satellite measurements, *Atmos. Chem. Phys.*, *10*, 6863–6872.

Kaufman, Y. J., D. Tanre, and O. Boucher (2002), A satellite view of aerosols in the climate system, *Nature*, *419*, 215–223.

Knippertz, P., and M. C. Todd (2012), Mineral dust aerosols over the Sahara: Meteorological controls on emission and transport and implications for modeling, *Rev. Geophys.*, *50*, RG1007, doi:10.1029/2011RG000362.

Lau, K. M., M. K. Kim, and K. M. Kim (2006), Asian summer monsoon anomalies induced by aerosol direct forcing: The role of the Tibetan Plateau, *Clim. Dyn.*, *26*, 855–864.

Liao, H., and J. H. Seinfeld (1998), Radiative forcing by mineral dust aerosols: Sensitivity to key variables, *J. Geophys. Res.*, *103*, 31,637–31,645, doi:10.1029/1998JD200036.

Liu, C. M., Z. A. Qian, M. C. Wu, M. H. Song, and J. T. Liu (2004), A composite study of the synoptic differences between major and minor dust storm springs over the China-Mongolia areas, *Terr. Atmos. Ocean. Sci.*, *15*, 999–1018.

Liu, Z., et al. (2008), Airborne dust distributions over the Tibetan Plateau and surrounding areas derived from the first year of CALIPSO lidar observations, *Atmos. Chem. Phys.*, *8*, 5045–5060.

Ramanathan, V., P. J. Crutzen, J. T. Kiehl, and D. Rosenfeld (2001), Atmosphere—Aerosols, climate, and the hydrological cycle, *Science*, *294*, 2119–2124.

Rosenfeld, D., Y. Rudich, and R. Lahav (2001), Desert dust suppressing precipitation: A possible desertification feedback loop, *Proc. Natl. Acad. Sci. U.S.A.*, *98*, 5975–5980.

Sassen, K., P. J. DeMott, J. M. Prospero, and M. R. Poellot (2003), Saharan dust storms and indirect aerosol effects on clouds: CRYSTAL-FACE results, *Geophys. Res. Lett.*, *30*(12), 1633, doi:10.1029/2003GL017371.

Shaw, W. J., K. J. Allwine, B. G. Fritz, F. C. Rutz, J. P. Rishel, and E. G. Chapman (2008), Evaluation of the wind erosion module in DUSTRAN, *Atmos. Environ.*, *42*, 1907–1921.

Su, J., J. Huang, Q. Fu, P. Minnis, J. Ge, and J. Bi (2008), Estimation of Asian dust aerosol effect on cloud radiation forcing using Fu-Liou radiative model and CERES measurements, *Atmos. Chem. Phys.*, *8*, 2763–2771.

Sun, J. M., M. Y. Zhang, and T. S. Liu (2001), Spatial and temporal characteristics of dust storms in China and its surrounding regions, 1960–1999: Relations to source area and climate, *J. Geophys. Res.*, *106*, 10,325–10,333, doi:10.1029/2000JD900665.

Tegen, I. (2003), Modeling the mineral dust aerosol cycle in the climate system, *Quat. Sci. Rev.*, *22*, 1821–1834.

Twohy, C. H., et al. (2009), Saharan dust particles nucleate droplets in eastern Atlantic clouds, *Geophys. Res. Lett.*, *36*, L01807, doi:10.1029/2008GL035846.

Uno, I., K. Eguchi, K. Yumimoto, T. Takemura, A. Shimizu, M. Uematsu, Z. Liu, Z. Wang, Y. Hara, and N. Sugimoto (2009), Asian dust transported one full circuit around the globe, *Nat. Geosci.*, *2*, 557–560.

Wang, X. M., Z. B. Dong, J. W. Zhang, and G. T. Chen (2002), Geomorphology of sand dunes in the Northeast Taklimakan Desert, *Geomorphology*, *42*, 183–195.

Winker, D. M., W. H. Hunt, and M. J. McGill (2007), Initial performance assessment of CALIOP, *Geophys. Res. Lett.*, *34*, L19803, doi:10.1029/2007GL030135.

Winker, D. M., M. A. Vaughan, A. Omar, Y. Hu, K. A. Powell, Z. Liu, W. H. Hunt, and S. A. Young (2009), Overview of the CALIPSO Mission and CALIOP data processing algorithms, *J. Atmos. Oceanic Tech.*, *26*, 2310–2323.

Yu, H., M. Chin, D. M. Winker, A. H. Omar, Z. Liu, C. Kittaka, and T. Diehl (2010), Global view of aerosol vertical distributions from CALIPSO lidar measurements and GOCART simulations: Regional and seasonal variations, *J. Geophys. Res.*, *115*, D00H30, doi:10.1029/2009JD013364.

Yumimoto, K., K. Eguchi, I. Uno, T. Takemura, Z. Liu, A. Shimizu, and N. Sugimoto (2009), An elevated large-scale dust veil from the Taklimakan Desert: Intercontinental transport and three-dimensional structure as captured by CALIPSO and regional and global models, *Atmos. Chem. Phys.*, *9*, 8545–8558.